Chapter 3

Determination of Design Parameters of a Dry Type Transformer using Finite Element Method

3.1   Introduction

The concept of dry type transformer is not new, however the enormous use of different types of insulating material in dry type distribution and power transformer makes it necessary to carry out the complete analysis of the transformer at the design stage to avoid probable failure in the field and consequently the power interruption and also to increase the cost effectiveness.

Finite Element Analysis (FEA) using Finite Element Method (FEM) was developed over 70 years to solve the complex elasticity and structural analysis problem in civil and aeronautical engineering. Application of FEA is being expanded to simulation in electrical engineering also to solve the complex design problems.   The circuit theory models for designing

transformers are not much accurate in determining the transformer parameters such as winding impedance, leakage inductance, hot spot temperature etc. The physical realization of these parameters is needed on a prototype unit. The finite element method can play a vital role in deriving these parameters without any physical verification. An effort has been made in this thesis to show the effectiveness of finite element method in determining the above said parameters while designing the transformers - for power and distribution sectors.

The hot spot in any electrical machine is due to losses in it. The hot spot temperature is to be determined for estimating the life of insulating material and consequently that of a machine. In a transformer the heat flow is in vertical direction through core and in horizontal and vertical direction through winding and insulation. It mainly depends on its geometry and type of construction. In a dry type transformer the construction is critical for maintaining the thermal capacity as the cooling media is air only. Thermal capacity is defined by its ability to supply the rated load within predefined temperature rise limit in connection with the temperature rise limits of the insulating materials used. The parameters governing the temperature rise are no load losses, load losses and the space between core and winding. The volume of core and winding plays a vital role in heat dissipation especially when cooling is only through natural air convection.

The another major problem observed during the design stage is the estimation of impedance value and short circuit forces in a transformer during dead short circuit on the load side of a transformer. The finite element analysis is to be done in determining such forces and also the impedance values to the close proximity there by reducing the design efforts.

The other type of short circuit in transformer is turn to turn, disk to disk or

turn/disk to earth short circuit. This occurs mainly because of the aging of the insulation. This leads to the overheating of the transformer and finally results into the transformer failure. Study shows that around 70-80% of the transformer failures are due to the short circuit between turns. Considering this damage occurring in the transformer and time and cost involved in rectifying the same, it seems that simulation involving modeling of the transformer is the most economical and convenient way.

The built-in leakage inductance of the transformer also helps in making them short circuit proof. The finite element analysis of a dry type transformer makes it possible to estimate winding reactance and leakage reactance to the close approximation [48] thereby reducing the design efforts for estimating the impedance value and also the short circuit forces.

Apart from above cited problems, the design of air distances (insulation supports) and exact estimation of magnetizing inrush current are major issues in oil cooled as well as dry type medium and high voltage transformers. However in oil cooled transformers the air distances are not creating havocs inside the transformer tank due to the presence of oil. But in dry type transformers this becomes a critical problem. Over dimensioning of air distances avoids the breakdown between upper high voltage side and core frame but at the same time adds to the cost and size of the transformer. Based on the estimation of the electric field distribution around the support and also around winding and core, the magnetizing inrush current can be computed to the closest approximation.

In this chapter an effort has been made to investigate on the core areas of dry type transformers (Distribution and Power Transformers of Medium Voltage range) as listed above with the help of finite element analysis.

3.2 Determination of Impedance Value and Estimation of Electromagnetic Forces under Short Circuit Condition

3.2.1 Short Circuit Current and Force Calculation

It is must to determine the impedance in a transformer to estimate the short circuit current and forces that may generate under short circuit condition. To find out the impedance value, it is required to have the value of resistance of the winding and reactance of the winding. The resistance value can be computed analytically by calculating the mean length of turn and cross section area of the conductor used. The reactance value based on the self inductance of coil can be computed by calculating the numbers of layers and total numbers of turns. The reactance value for concentric cylindrical coils having equal length of primary and secondary windings can be computed using equation 3.1 [119].

$$X = 2\pi f \mu_0 T^2 \frac{L_{mt}}{L_C}(a + (\frac{b1 + b2}{3})) \tag{3.1}$$

Where

T = No. of turns of respective winding (HV or LV winding)

L_{mt} = Mean length of turn of respective winding

L_C = Length of coil

a = Thickness of duct between HV and LV winding

$b1$ = Thickness of HV winding

$b2$ = Thickness of LV winding

However, this does not give the actual estimation of mutual reactance and hence the actual value of impedance. This increases the difficulties in

computing the actual short circuit current and short circuit forces. Also, involvement of the magnetic path (core) increases the complexity further as it changes the leakage flux levels.

As an alternative, the short circuit forces can be estimated quite accurately by determining the electric field intensity along the various segments of the winding using Finite Element Method (FEM). The Lorentz's force due to short circuit current and linkage flux causes mechanical forces and deformation in the winding. To estimate the resultant mechanical forces on the winding, a sequential FEM as presented in [4] has been used. The flow chart for the same is shown in Figure 3.1.

The short circuit current under transient condition can be approximated as

$$I_{sc(t)} = I_0 e^{-\frac{R}{L}t} + \frac{Vm}{\sqrt{R^2 + X^2}} cos\ \omega t \qquad (3.2)$$

Where,
I_{sc} = the short circuit current in Ampere (A)
I_0 = the initial current in Ampere (A)
R , L and X are resistance in Ohm (Ω) ,Inductance in Henry (H) and reactance in Ω respectively.

The value of initial current depends on the instant of switching the circuit. At switching instant $t = 0$, if voltage is zero then I_0 will have maximum value and if voltage is at its peak then it will be zero. The transient magnetic flux depends on the magnetizing characteristics. Since this is an air core reactor, the linking flux will increase in proportion to the short circuit current. The component of the flux using vector potential can be expressed as
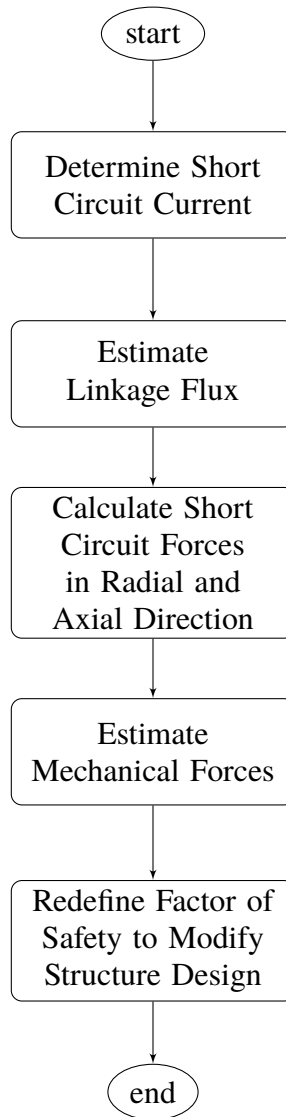
```
                    ┌─────────┐
                    │  start  │
                    └─────────┘
                         │
                         ▼
              ┌────────────────────┐
              │  Determine Short   │
              │  Circuit Current   │
              └────────────────────┘
                         │
                         ▼
              ┌────────────────────┐
              │     Estimate       │
              │   Linkage Flux     │
              └────────────────────┘
                         │
                         ▼
              ┌────────────────────┐
              │  Calculate Short   │
              │  Circuit Forces    │
              │   in Radial and    │
              │  Axial Direction   │
              └────────────────────┘
                         │
                         ▼
              ┌────────────────────┐
              │     Estimate       │
              │ Mechanical Forces  │
              └────────────────────┘
                         │
                         ▼
              ┌────────────────────┐
              │ Redefine Factor of │
              │  Safety to Modify  │
              │  Structure Design  │
              └────────────────────┘
                         │
                         ▼
                    ┌─────────┐
                    │   end   │
                    └─────────┘
```

Figure 3.1: Flow Chart for Short Circuit Analysis

$$B_r = \frac{\partial A_\phi}{\partial z}, \quad B_\phi = 0, \quad B_z = \frac{1}{r}\frac{\partial r A_\phi}{\partial z} \tag{3.3}$$

According to Lorentz's force, the expression for electromagnetic force is given as in equation 3.4. It is unidirectional pulsating type since it is proportional to the square of the current.

$$\overrightarrow{F_t} = F_m \left(\frac{1}{2} + e^{-\frac{2R}{L}t} - 2\,e^{-\frac{R}{L}t}cos\ \omega t + \frac{1}{2}cos\ 2\omega t \right) \tag{3.4}$$

Where ,

$\overrightarrow{F_t}$ = the electromagnetic force in Newton (N) at any instant t

F_m = the maximum value of force in N

This force $\overrightarrow{F_t}$ comprises of two forces, one in radial direction and other in axial direction.

3.2.2   Determination of Stresses in a Model Coil using FEA

To determine radial (Transverse) and axial (Longitudinal) forces on a prototype coil, the model of an air core reactor was selected as shown in Figure 3.2 with the specifications as given in Table 3.1. For better estimation of the impact of axial forces, two reactor coils have been placed one over the other. The reactor is consisting of one single coil only and hence the radial force will be in outward direction.

The axial force will be having predominant effect in the downward direction for bottom coil and in the upward direction for top coil. This is because the stack of these coils is to be connected with one single phase only. The
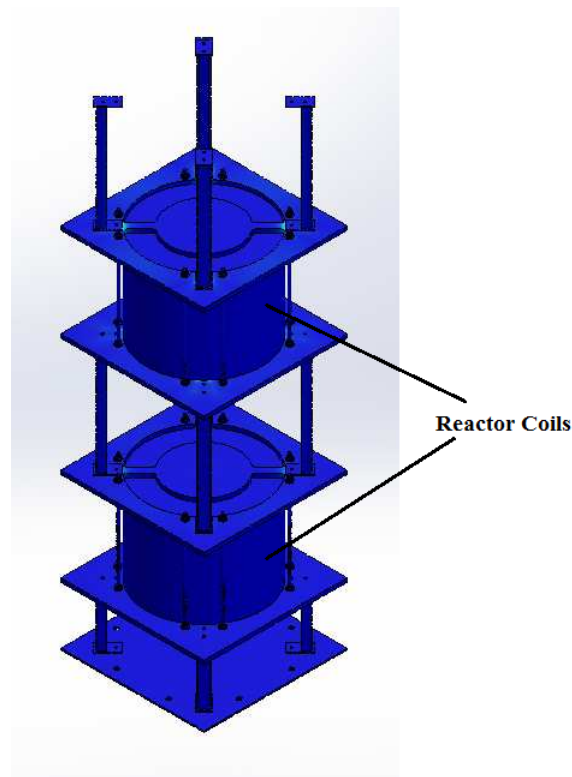
Figure 3.2: Reactor Model

Table 3.1: Specifications of Air Core Reactor

Type of Reactor	Air Core Dry Type
Category	Series Reactor
Line Voltage	600 V
Current Rating	500 A
Duty	Continuous
Thermal Short Circuit Ability	16 Times Rated Current For 2 sec
Reference Standard	IEC 60076-6, 2007

maximum calculated value of radial force found is 605 N and that of axial force is 363 N. To find out the structural deformation, these forces are used as an input data to the stress strain model using von Mises Criterion.

3.2.3   Stress Strain Calculation and Deformation Prediction

The von Mises yield criterion is used to determine the stress level in the reactor coil during short circuit condition. Mathematically the von Mises yield criterion is expressed as:

$$J_2 = K^2 \tag{3.5}$$

stress in pure shear is $\sqrt{3}$ times lower than the tensile yield stress in the case of simple tension. Thus, we have

$$K = \frac{\sigma_y}{\sqrt{3}} \tag{3.6}$$

Where
σ_y = the yield strength of the material.

If we set the von Mises stress equal to the yield strength and combine the above equations, the von Mises yield criterion can be expressed as:

$$\sigma_v = \sigma_y = \sqrt{3J_2} \tag{3.7}$$

In terms of Cauchy's stress tensor components, this criterion can be expressed as

$$\sigma_v^2 = \frac{1}{2} \left[(\sigma_{11} - \sigma_{22})^2 + (\sigma_{22} - \sigma_{33})^2 + (\sigma_{33} - \sigma_{11})^2 + 6 \left(\sigma_{12}^2 + \sigma_{23}^2 + \sigma_{31}^2 \right) \right]$$

(3.8)

This equation 3.8 defines the yield surface as a circular cylinder whose intersection with the deviatoric (π)plane is a circle. It can be reduced and reorgnized for practical use in different loading conditions.

In case of uni-axial stress or simple tension, $\sigma_1 \neq 0$, and $\sigma_2 = \sigma_3 = 0$ then the von Mises criterion simply reduces to $\sigma_1 = \sigma_y$ which means that the material starts to yield when normal stress (uni-axial stress) reaches the yield strength of the material.

Using the results obtained from simple uni-axial tensile tests, yielding of material can be predicted under multi-axial loading conditions. In this situation, the equivalent tensile stress or von Mises stress σ_v can be expressed as in equation 3.9.

$$\sigma_v^2 = \frac{1}{2} \left[(\sigma_1 - \sigma_2)^2 + (\sigma_2 - \sigma_3)^2 + (\sigma_3 - \sigma_1)^2 \right]$$ (3.9)

The short circuit forces calculated above are converted into equivalent mechanical load with an adequate factor of safety (SF). The stress/strain values are then computed using von Mises criterion. The stress and strain values have been calculated for the following conditions.

1. Transverse (horizontal/radial) load and Longitudinal (vertical/axial) load with a factor of safety 1.5.

2. Axial and radial load with increased factor of safety (SF 2) by strengthening the mechanical structure and coil supports.

Table 3.2: Boundary Conditions

Load Pattern	No. of Nodes	No. of Elements	Boundary Conditions	
			Total Stress in MPa	Total Deformation in mm
Transverse	230029	690087	≤ 270	≤ 2.0
Longitudinal	243154	729462	≤ 70	≤ 1.0

3.2.4   Stress and Deformation with Factor of Safety 1.5 for Transverse and Longitudinal Loading

The determination of factor of safety is done based on the average value of force calculated and stress likely to be exerted on the available surface area of the support structure. It is the ratio of yield stress to the actual stress.

The boundary conditions for these entire analysis are as shown in Table 3.2. The Stress, Strain and Deformation values are summerized in Table 3.3 for a safety factor of 1.5. The values shown are the maximum values obtained during the analysis at a particular node. The safety factor of 1.5 has been chosen arbitrarily to have an initial start. There is no restriction in choosing the safety factor. The boundary values for stresses per unit area have been obtained using equations 3.10 and 3.11 for Transverse and Longitude forces (stresses) respectively [119].

$$\sigma_r = \frac{1}{2}\mu_0(iT^2)(\frac{L_{mt}}{L_c}) \tag{3.10}$$

$$\sigma_a = \frac{1}{2}\mu_0(iT^2)(\frac{L_{mt}}{(2(a + b_1 + b_2))}) \tag{3.11}$$

Figures 3.3, 3.4, 3.5 and 3.6 are showing the stress and deformation values in various segments of reactor coil assembly in Transverse and Longitudinal loading with safety factor of 1.5 respectively.

Table 3.3: Stress Strain Values and Deformation for SF 1.5

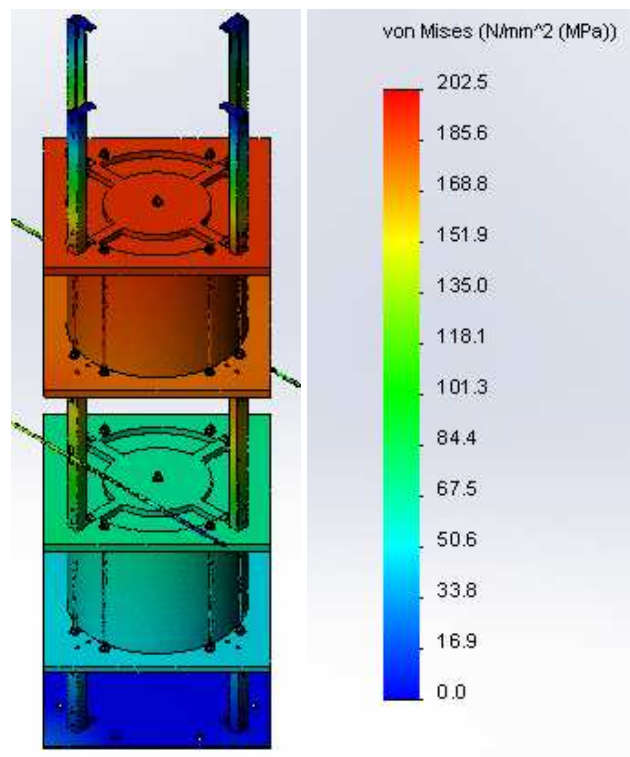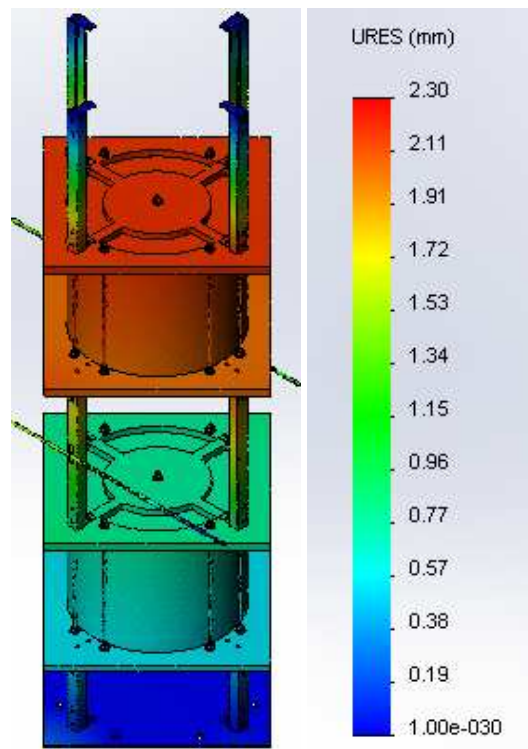| Load Pattern	Stress in MPa	Strain $\times 10^{-3}$	Deformation in mm
Transverse	202.5	4.692	2.300
Longitudinal	74.4	3.560	0.710

Figure 3.3: Stress with Transverse Loading. SF-1.5

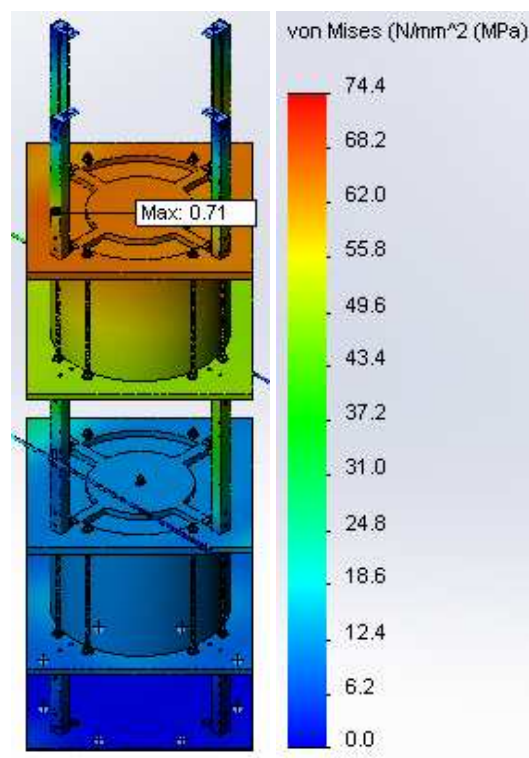Figure 3.4: Deformation with Transverse Loading. SF-1.5

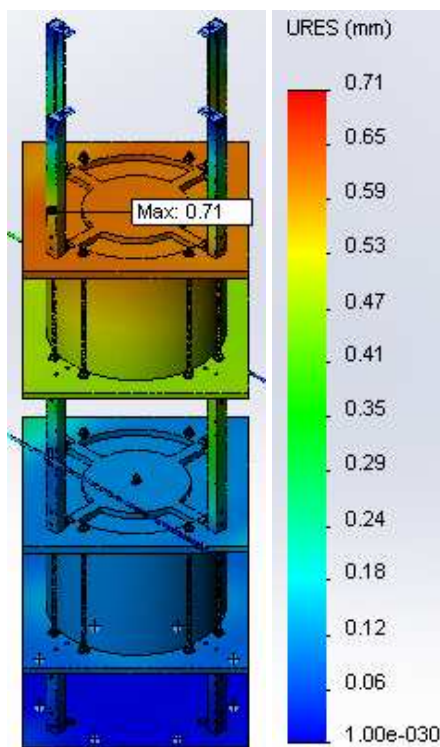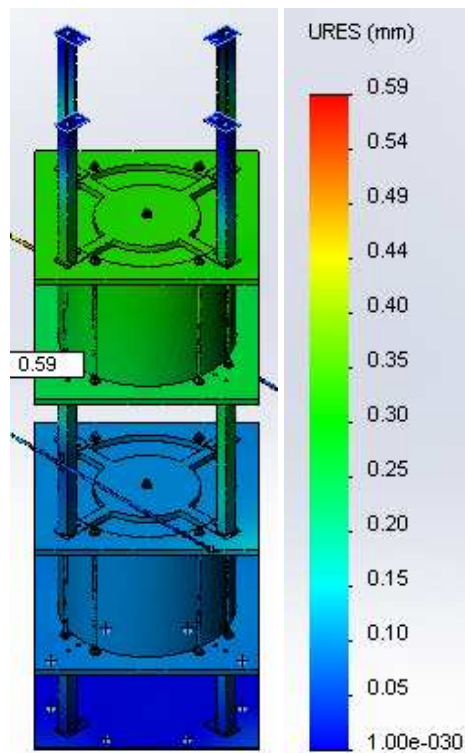Figure 3.5: Stress with Longitudinal Loading. SF-1.5

Figure 3.6: Deformation with Longitudinal Loading. SF-1.5

3.2.5   Stress and Deformation with Factor of Safety 2.0 for Transverse and Longitudinal Loading

Based on the results obtained for a safety factor of 1.5, it was decided to increase it to 2 as in Longitudinal loading with a safety factor of 1.5, the stress developed has crossed the boundary condition limit of 70 MPa whereas the deformation obtained in Transverse loading has also crossed the boundary condition limit of 2.0 mm. For achieving higher safety factor, the thickness of the support plate has been increased to meet longitudinal need and horizontal cross struss have been added to meet the transverse need. Also the size of the wire gauge has been increased so as to complete the layer and to make the winding more capable for handling thermal stresses which have not been takene into account during the entire analysis.

The results showing the maximum values of stress strain and deformation with safety factor 2.0 are summarized in Table 3.4. Figures 3.7, 3.8, 3.9
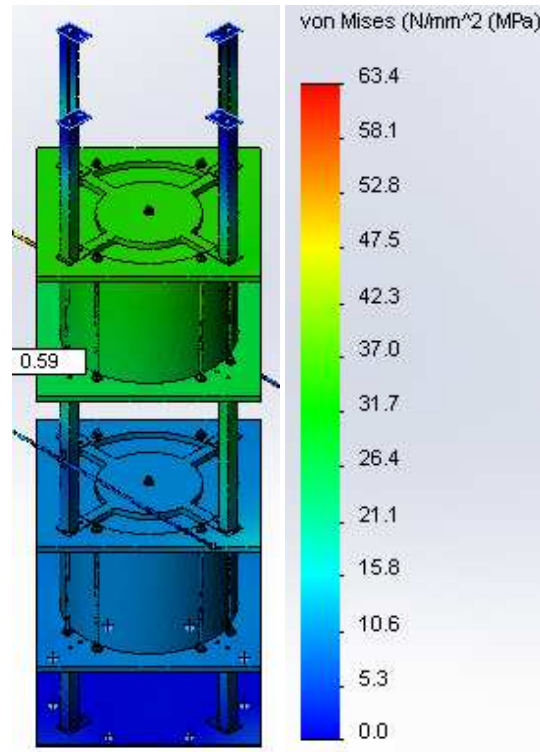
Figure 3.7: Stress with Transverse Loading. SF-2

Table 3.4: Stress Strain Values and Deformation for SF 2

Load Pattern	Stress in MPa	Strain $\times 10^{-3}$	Deformation in mm
Transverse	63.4	2.136	0.590
Longitudinal	27.1	3.000	0.601

and 3.10 are showing the stress and deformation values in various segments of reactor coil assembly in Transverse and Longitudinal loading with safety factor of 2 respectively.

In this analysis, the effect of thermal stresses due to heat generated during short circuit condition has not been taken into account due to the fact that the testing at 16 times rated current will be for 2 seconds only and being a thermal short circuit test, there will not be any consecutive shots for which thermal effects are needed to be accounted for. Also the current density taken is less than 1 Ampere/square mm.

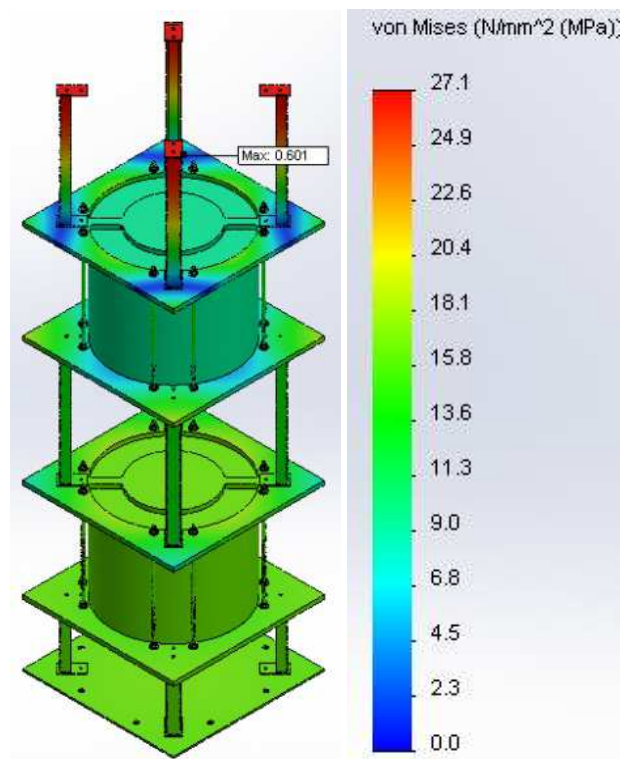Figure 3.8: Deformation with Transverse Loading. SF-2

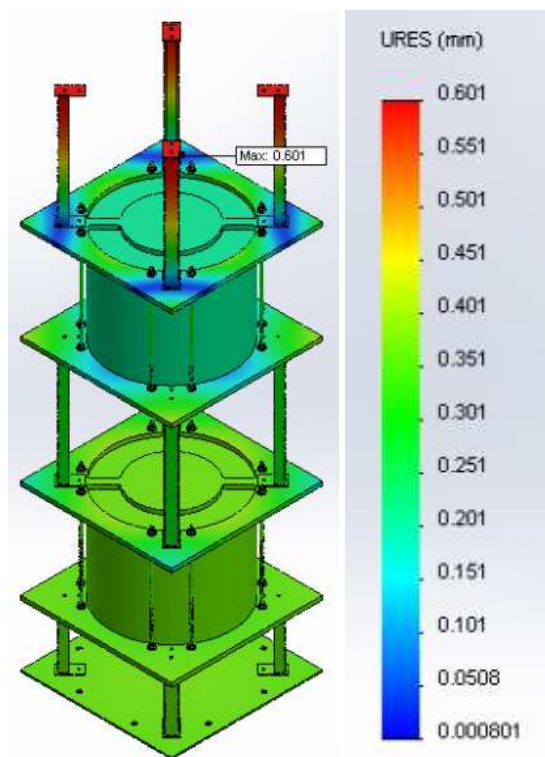Figure 3.9: Stress with Longitudinal Loading.SF-2

Figure 3.10: Deformation with Longitudinal Loading.SF-2

3.2.6   Results

The summary of the results obtained using the FEM by applying von Mises criterion is given in Table 3.4 for a safety factor of 2. Above results shows that with increased value of safety factor, the stress value in Transverse loading and deformation therein have reduced substantially. This indicates that with strengthening of mechanical structure and coil supports, the geometry has become more rigid to sustain the electromagnetic forces. Based on the above results, the reactor coil was subjected to the actual thermal short circuit test at CPRI, Bhopal, India.

A Short circuit current of value 8000 A rms was passed for 2 second. The reactor coil withstood the current successfully. The passing criteria was – "variation in inductance value of the reactor must be within +/- 2% of the design/declared value". At the end of test, the variation in inductance value

found was 0.081%, which was quite below 2%. Thus it successfully passed the test.

Based on above results, the geometry of the coil has been freezen and the actual value of impedance (reactance) is computed using equation 3.1.

3.3   Determination of Temperature Rise

3.3.1   Thermal Capacity of a Dry Type Transformer

The hot spot in any electrical machine is due to losses in it. The hot spot temperature is to be determined for estimating the life of the insulating material and consequently that of a machine. In a transformer the heat flow is through core in verical direction and to winding and insulation in horizontal direction.   It mainly depends on its geometry and type of construction.

In a dry type transformer the construction is critical for maintaining the thermal capacity. Thermal capacity is defined by its ability to supply the rated load within predefined temperature rise limit in connection with the temperature rise limits of the insulating materials used. The parameters governing the temperature rise are no load losses, load losses and the space between core and winding. The volume of core and winding plays a vital role in heat dissipation.

3.3.2   Heat Dissipation in Core

The transformer core consists of silicon steel laminations insulated from each other having thickness varying from 0.5 mm to 0.23 mm or even less. Due
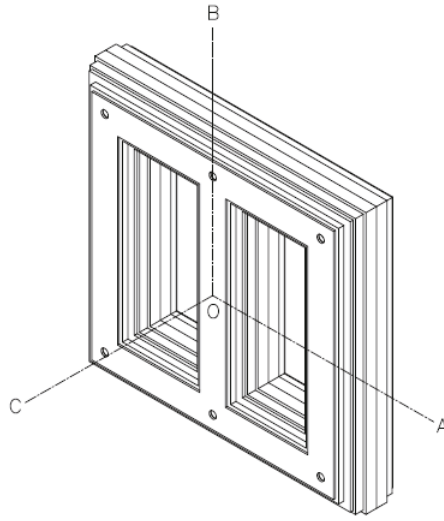
Figure 3.11: Elementary Core Model

to alternate magnetization of the core, iron losses take place which in turn produces heat.

Figure 3.11 shows an elemental core of a transformer. The centre of the core is its hottest part. The heat dissipation will be through conduction at surfaces A (heat flow along X axis across the lamination) and B (heat flow along Z axis along the lamination) and through convection in direction C (Y axis).

The temperature of the hottest spot is described as [118] [120]

$$\theta_m = \frac{q\rho t^2}{8} + \theta_s \tag{3.12}$$

Where,
q = the heat produced per unit volume in W/m^3
t = the lamination thickness in m
ρ = the thermal resistivity of the material along the direction of heat flow in $^\circ C\ m/W$
θ_s = the initial surface temperature of the core in $^\circ C$

The temperature gradient along A, B and C directions can be expressed as

$$\theta_a = \frac{q\rho_a t^2}{2}, \qquad \theta_b = \frac{q\rho_b t^2}{2}, \qquad \theta_c = \frac{q\rho_c t^2}{2} \qquad (3.13)$$

Where,

ρ_a, ρ_b and ρ_c are the thermal resistivity of the lamination across the core, along the core and that of air respectively.

Though the thermal resistivity along the core is quite low, the heat dissipation along the core is not effective as the height of the core is quite large as compared to the thickness. This becomes more critical especially when the coil/winding construction is concentric layer type.

Also the thermal resistivity of air is quite large which does not help significantly in heat dissipation. The effective heat dissipation is across the lamination and because of the air flow through the ventilating duct either on the periphery of the core or within the core placed axially as per design requirement.

3.3.3   Heat Dissipation in Winding and Insulation

The transformer windings are consisting of non-homogenous surfaces and hence heat dissipation is not uniform and does not take place along the parallel paths only. As the windings have insulation in addition to Copper or Aluminium i.e. conductor, the thermal resistivity of built up windings depends upon the relative thickness of insulation to conductor. The heat flow in a winding normally takes place in two directions – radially and axially outwards.

The hot spot temperature in a transformer winding with square/rectangular geometry can be estimated by equation 3.14 and for cylindrical geometry by equation 3.15, [118].

$$\theta_{sr} = \frac{q\ell\omega t}{8\ell \left[\frac{\omega}{t\rho_x} + \frac{t}{\omega\rho_y} \right]} \tag{3.14}$$

Where,

ℓ = the length (height) of the coil in m,

t = the thickness of the coil in m,

w = the width or outer diameter of the coil in m ,

ρ_x and ρ_y = thermal resistivity in radial and axial directions respectively in $°C\ m/W$

$$\theta_{cy} = \frac{q\rho_{co}t^2}{2} \tag{3.15}$$

Where,

$\rho_{co} = \rho_i \left(1 - s_f^{0.5} \right)$ =thermal resistivity of coil in $°C\ m/W$

ρ_i = thermal resistivity of insulating material

S_f= Space factor = conductor area/total winding area

While determining the hot spot temperature of a winding, one must consider the effect of momentary overloads to which the transformer is being subjected during its entire life span.   For such overloads the temperature is calculated with assumption that all the heat developed is stored in the conductor without dissipation. The temperature rise is then calculated using equation 3.16 [119].

$$\theta = \alpha t \left\{ \frac{2T1 + \alpha t}{2T1} + \frac{620 K_d}{2T1 + \alpha t} \right\} \tag{3.16}$$

Where,

t = overload duration in second

$T_1 = \theta_1 + 234.5^\circ C$

θ_1= Initial temperature in $^\circ C$

α = 0.0025*Total $I^2 R$ losses in W/kg at θ_1

K_d = Eddy current ratio at $75^\circ C$ = Actual $I^2 R$ loss / DC $I^2 R$ loss

To estimate the hot spot temperature in the winding, due to combined effect of core losses and winding losses a FEM based on [26] [57] [59] is used. The flow chart for this is given in Figure 3.12

3.3.4   Heat Transfer Calculation using FEA

The heat conduction in an orthotropic solid body is governed by the differential equation [117] that is expressed as:

$$\frac{\partial}{\partial x} \left(k_x \frac{\partial T}{\partial x} \right) + \frac{\partial}{\partial y} \left(k_y \frac{\partial T}{\partial y} \right) + \frac{\partial}{\partial z} \left(k_z \frac{\partial T}{\partial z} \right) + q^{'} = \rho c \frac{\partial T}{\partial t} \tag{3.17}$$

Where,

k_x, k_y, k_z are the thermal conductivities of the material in x, y and z direction respectively, T is the temperature, ρ is the density of the material, c is the specific heat of the material and q' is the rate of heat generated per unit volume.

Considering thermal conductivity in all the direction to be same, i.e $k_x, k_y, k_z = k$, equation 3.17 reduces to
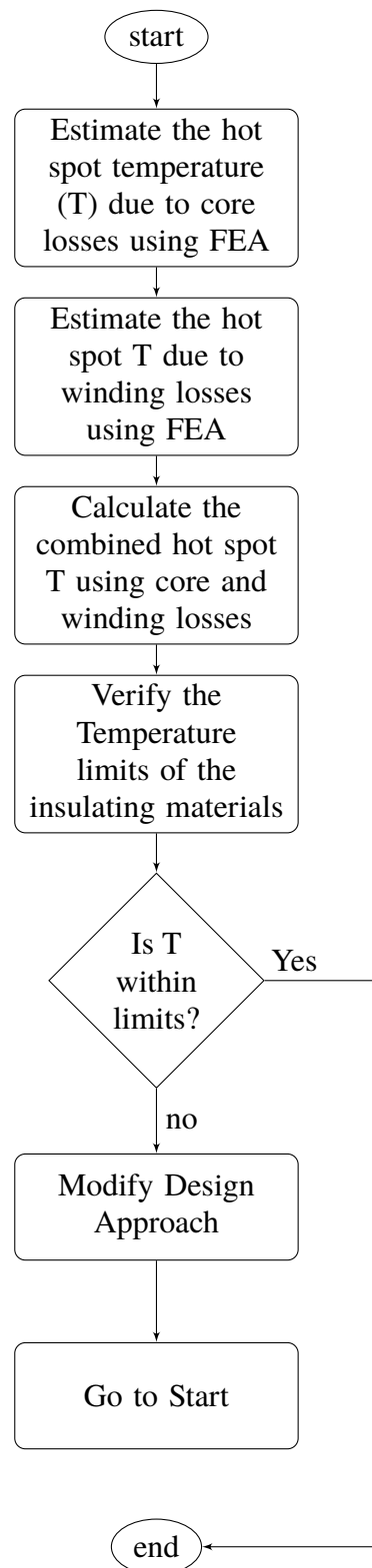
start

Estimate the hot spot temperature (T) due to core losses using FEA

Estimate the hot spot T due to winding losses using FEA

Calculate the combined hot spot T using core and winding losses

Verify the Temperature limits of the insulating materials

Is T within limits?

Yes

no

Modify Design Approach

Go to Start

end

Figure 3.12: The Flow Chart for Thermal Analysis of Transformer

$$\frac{\partial^2 T}{\partial x^2} + \frac{\partial^2 T}{\partial y^2} + \frac{\partial^2 T}{\partial z^2} + \frac{q'}{k} = \frac{1}{\alpha}\frac{\partial T}{\partial t} \tag{3.18}$$

Where,

$\alpha = \frac{k}{\rho c}$ known as thermal diffusivity.

Equation 3.18 is the equation for heat conduction which governs the distribution of temperature and the heat flow due to conduction in a solid with uniform material properties (isotropic body).

If body does not contain any heat source then equation 3.18 changes to the Fourier equation,

$$\frac{\partial^2 T}{\partial x^2} + \frac{\partial^2 T}{\partial y^2} + \frac{\partial^2 T}{\partial z^2} = \frac{1}{\alpha}\frac{\partial T}{\partial t}. \tag{3.19}$$

When the body is having heat sources and is in a steady state, equation 3.18 becomes the Poisson's equation,

$$\frac{\partial^2 T}{\partial x^2} + \frac{\partial^2 T}{\partial y^2} + \frac{\partial^2 T}{\partial z^2} + \frac{q'}{k} = 0 \tag{3.20}$$

And when the body is without any heat source and is in a steady state, equation 3.18 becomes the Laplace equation,

$$\frac{\partial^2 T}{\partial x^2} + \frac{\partial^2 T}{\partial y^2} + \frac{\partial^2 T}{\partial z^2} = 0 \tag{3.21}$$

Two boundary conditions required to be specified as the differential equations 3.18 or 3.19 - is of second order. The possible conditions are

$$T(x, y, z, t) = T_0 \quad for \; t{>}0 \; on \; S_1 \tag{3.22}$$

$$k_x \frac{\partial T}{\partial x} l_x + k_y \frac{\partial T}{\partial y} l_y + k_z \frac{\partial T}{\partial z} l_z + q_0 = 0 \quad for\ t{>}0\ on\ S_2 \qquad (3.23)$$

$$k_x \frac{\partial T}{\partial x} l_x + k_y \frac{\partial T}{\partial y} l_y + k_z \frac{\partial T}{\partial z} l_z + h\left(T - T_\infty\right) = 0 \quad for\ t{>}0\ on\ S_3 \quad (3.24)$$

Where,

q_0 is the heat flux at boundary, h is the heat transfer coefficient due to convection, T_∞ is the temperature of surroundings and l_x, l_y, l_z are the direction cosines of the outward drawn normal to the boundary.

The boundary condition as in equation 3.22 is applicable when the surface is self heating or in contact with melting solid or a boiling liquid, the second condition as in equation 3.23 is applicable when a thin film or patch heater is attached to the surface and the third condition as in equation 3.24 is applicable when cold or hot air flows around the surface.

Equation 3.18 or 3.19 is a first order equation in time t, and hence one initial condition is required, which is expressed as

$$T(x, y, z, t) = \overline{T_0}(x, y, z) in V \qquad (3.25)$$

Where,

V is the domain (volume) of the solid body and $\overline{T_0}$ is the specified temperature distribution at time zero.

In present work, the finite element equations for the heat conduction problem have been derived using a 3D Variational approach.   The temperature distribution T(x, y, z, t) has been found inside the solid body by

minimizing the integral function as shown in equation 3.26 that satisfies all boundary conditions and initial condition stated in equations 3.22 to 3.25.

$$
I = \frac{1}{2} \int \int \int_V
$$
$$
\left[k_x \left(\frac{\partial T}{\partial x} \right)^2 + k_y \left(\frac{\partial T}{\partial y} \right)^2 + k_z \left(\frac{\partial T}{\partial z} \right)^2 - 2 \left(q' - \rho c \underbrace{\frac{\partial T}{\partial t}} T \right) \right] dV \tag{3.26}
$$

$$
+ \int \int_{s_2} q_0 T ds_2 + \frac{1}{2} \int \int_{s_3} h(T - T_\infty)^2 ds_3
$$

The step wise procedure involved in deriving the finite element equations is given below.

Step 1: Domain V is to be divided into E finite elements each having p nodes.

Step 2: Estimate the variation of T in each finite element with a suitable form and express it in element e as

$$
T^{(e)}(x, y, z, t) = [N(x, y, z)] \vec{T}^{(e)} \tag{3.27}
$$

Where,

$$
[N(x, y, z)] = [N_1(x, y, z) \quad N_2(x, y, z) .... N_p(x, y, z)]
$$

$$
\vec{T}^{(e)} = \left\{ \begin{array}{c} T_1(t) \\ T_2(t) \\ . \\ . \\ . \\ T_p(t) \end{array} \right\}^{(e)}
$$

$T_i(t)$ is the temperature of node i and N_i (x, y, z) is the interpolation function corresponding to node i of element e.

Step 3: The functional I is to be expressed as a sum of E elemental quantities $I^{(e)}$ as

$$I = \sum_{e=1}^{E} I^{(e)} \tag{3.28}$$

Where,

$$I^{(e)} = \frac{1}{2} \int \int \int_V$$

$$\left[k_x \left(\frac{\partial T^{(e)}}{\partial x} \right)^2 + k_y \left(\frac{\partial T^{(e)}}{\partial y} \right)^2 + k_z \left(\frac{\partial T^{(e)}}{\partial z} \right)^2 - 2 \left(q' - \rho c \underbrace{\frac{\partial T^{(e)}}{\partial t}} T^{(e)} \right) \right] dV$$

$$+ \int \int_{s_2} q_0 T^{(e)} ds_2 + \frac{1}{2} \int \int_{s_3} h(T^{(e)} - T_\infty)^2 ds_3$$

$$\tag{3.29}$$

For the minimization of the functional I, use the necessary conditions

$$\frac{\partial I}{\partial T_i} = \sum_{e=1}^{E} \frac{\partial I^{(e)}}{\partial T_i} = 0 \qquad i = 1, 2, ...M \tag{3.30}$$

Where, M is the total number of nodal temperature unknowns.

Equations 3.29 and 3.30 can be further simplified to equation 3.31 with a note that if node i does not lie on S_2 and S_3 then the surface integrals will not appear

$$\frac{\partial I^{(e)}}{\partial \vec{T}_i^{(e)}} = \left[K_1^{(e)} \right] \vec{T}^{(e)} - \vec{P}^{(e)} + \left[K_2^{(e)} \right] \vec{T}^{(e)} + \left[K_3^{(e)} \right] \vec{T}^{(e)} \qquad (3.31)$$

Step 4: Rewrite equation 3.31 in matrix form as

$$\frac{\partial I}{\partial \vec{T}} = \sum_{e=1}^{E} \frac{\partial I^{(e)}}{\partial \vec{T}^{(e)}}$$

$$= \sum_{e=1}^{E} \left[K_1^{(e)} \right] \vec{T}^{(e)} - \vec{P}^{(e)} + \left[K_2^{(e)} \right] \vec{T}^{(e)} + \left[K_3^{(e)} \right] \vec{T}^{(e)} = \vec{0}$$

$$(3.32)$$

Where, $\vec{T}$ is the vector of unknown nodal temperatures of the system.

$$\vec{T} = \left\{ \begin{array}{c} T_1 \\ T_2 \\ . \\ . \\ . \\ T_p \end{array} \right\}$$

Using familiar assembly process, equation 3.32 can be expressed as

$$\left[K_3 \right] \vec{T} + \left[K \right] \vec{T} = \vec{P} \qquad (3.33)$$

Where ,

$$\left[\underbrace{K}_{3} \right] = \sum_{e=1}^{E} \left(\left[K_{3}^{(e)} \right] \right) \tag{3.34}$$

$$\left[\underbrace{K} \right] = \sum_{e=1}^{E} \left(\left[K_{1}^{(e)} \right] + \left(\left[K_{2}^{(e)} \right] \right) \right) \tag{3.35}$$

$$\underbrace{\vec{P}} = \sum_{e=1}^{E} (\vec{P}^{(e)}) \tag{3.36}$$

Step 5: Equations 3.33 to 3.36 are the equations those have to be solved after incorporating the specified boundary conditions over S_1 of equation 3.22 and the initial conditions of equation 3.25.

3.3.5   Estimation of Temperature Rise in Model transformer

3.3.5.1   Design Approach A

The transformer model has been shown in Figure 3.13 and its specifications are as given in Table 3.5, for which the temperature distribution in core and winding has been estimated using 3D approach described above and overall temperature rise has been calculated.

The FEA has been carried out with the use of eight node brick element approach [111] and [113] where each of the eight nodes has single translational degrees of freedom in the nodal x, y or z directions. For carrying these entire analysis, the initial and boundary conditions used are used as shown in Table 3.6. The boundary conditions are indicating the maximum temperature limits considering the combined effects of core
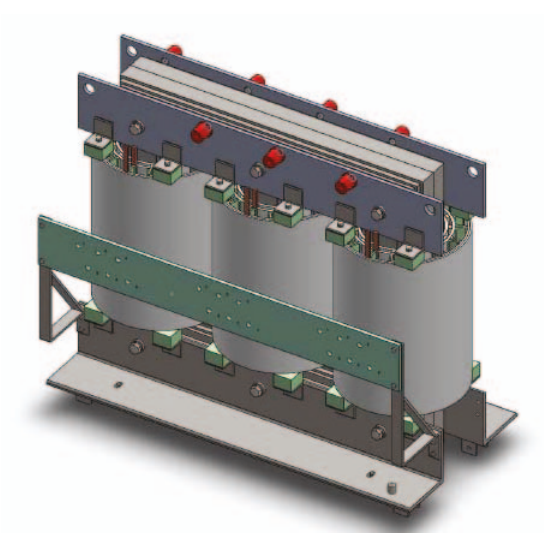
Figure 3.13: Transformer Model

Table 3.5: Specification of 160 kVA Transformer

Types of Transformer	Dry type Double Wound
Rating	160 kVA,50Hz,3 Phase
Impregnation	Vacuum Pressure Impregnated
Insulation Class	H
Input/Output Voltage	415 V (Delta) / 415 V (Star)
Impedance	4 %
Duty/ Vector Group	Continuous/Dyn1
Core/Copper Losses	1000 / 2400 at $75°$ C in W (Max)
Temperature Rise Limit	$70°$ C (Within Insulation Class B limit)
Reference Standard	IS 11171/2026

Table 3.6: Initial & Boundary Conditions

Segment Analysis	Number of Element	Initial Condition	Boundary Condition
		Initial Temp. in $°$ C	Hot Spot Temp. of Winding in $°$ C
Core	240060	35	$\leq 22 + 50^*$
Windings	276099	35	$\leq 58 + 50^*$
Complete Assembly	-	-	$\leq 70 + 50^*$
* 50 is the design ambient temperature in $°C$			
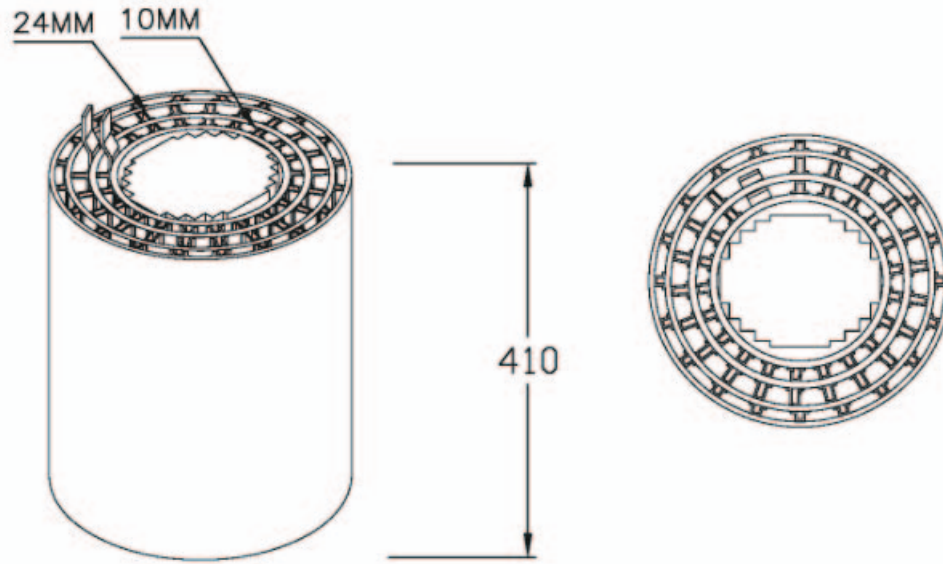
Figure 3.14: Coil Geometry A

Table 3.7: Design Approach A

Flux Density	1.3 $Tesla$
Tesla Winding ID	210 mm
Current Density – Secondary (Inner) Windings	1.8 A/mm^2
Current Density – Primary (Outer) Windings	2.5 A/mm^2
Spacer Size	10/24 mm

losses and winding losses. The analysis has been carried out for design approach A as shown in Table 3.7 in accordance to the simulation load method of IS 11171: 1985 to have better comparision with the practical method.

The values of winding temperature are summerized in Table 3.8 for coil geometry A as shown in Figure 3.14. The values indicated are the maximum values found during the analysis at a particular node after segmentized analysis of core and winding for their specified losses respectively. The total temperature rise of the winding as a compelte assembly is calculated using equation 3.37.

Table 3.8: Temperature Rise for Coil Geometry A

Segment Analyzed	Temperature Rise of Winding in $^\circ$ C					
	U1	V1	W1	U2	V2	W2
Core	7.8	8.5	8.2	24.5	24.7	24.8
Windings	56.0	57.2	57.0	62.0	62.5	62.8
Complete Assembly	59.8	61.4	61.0	77.1	77.7	78.1

$$\theta_T = \theta_c \left[1 + \left(\frac{\theta_e}{\theta_c} \right)^{1.25} \right]^{0.8} \tag{3.37}$$

Where,

θ_T=the total temperature rise of the winding

θ_e=the temperature rise of the winding due to no load losses

θ_c=the temperature rise of the winding due to I^2R losses.

3.3.5.2   Design Approach B

Based on the results obtained, it was decided to change the design parameters to have better air circulation in actual condition. Approach B has been adopted for further analysis as shown in Table 3.9. The coil geometry for the same has been shown in Figure 3.15.

The values of temperature rise based on the hot spot temperatures are summarized in Table 3.10 below and the temperature distribution of complete assembly for all the three phases of primary and secondary windings have been shown in Figures 3.16 and 3.17. The ambient temperature of 35 $^\circ C$ has been considered during all these calculations.

In this analysis while deriving the hot spot temperatures, the effect of surrounding ambient temperature on heat dissipation as well as the effect of
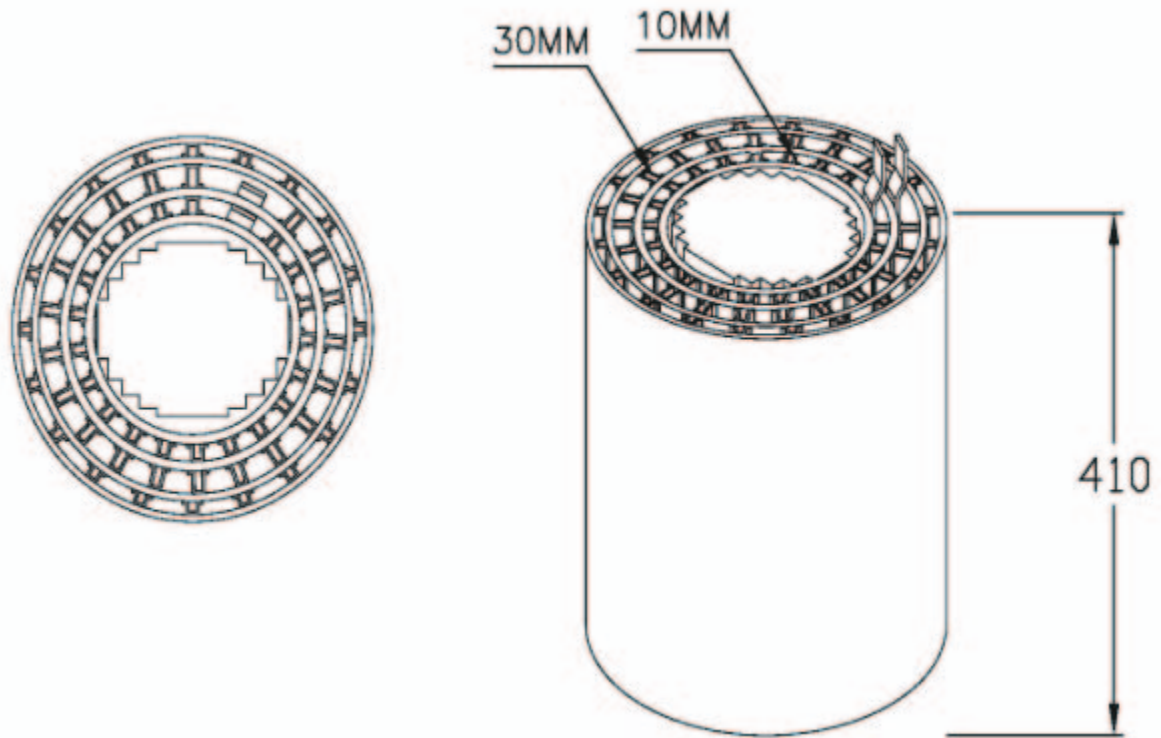
Figure 3.15: Coil Geometry B

Table 3.9: Design Approach B

Flux Density	1.275 $Tesla$
Tesla Winding ID	215 mm
Current Density – Secondary (Inner) Windings	1.8 A/mm^2
Current Density – Primary (Outer) Windings	2.5 A/mm^2
Spacer Size	10/30 mm

Table 3.10: Temperature Rise for Coil Geometry B

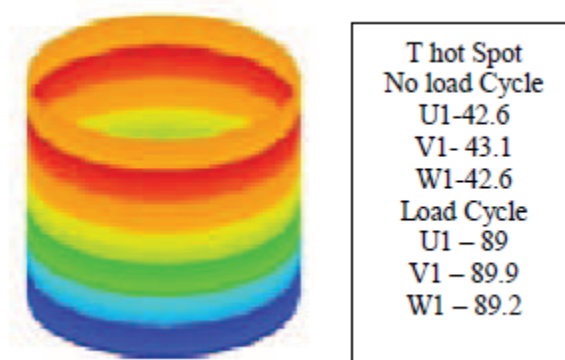| Segment Analyzed	Temperature Rise of Winding in $^\circ$ C					
	U1	V1	W1	U2	V2	W2
Core	7.6	8.1	7.9	23.5	23.7	23.5
Windings	54.0	54.9	54.2	49.2	49.7	49.4
Complete Assembly	57.7	58.9	58.1	64.3	64.9	64.5

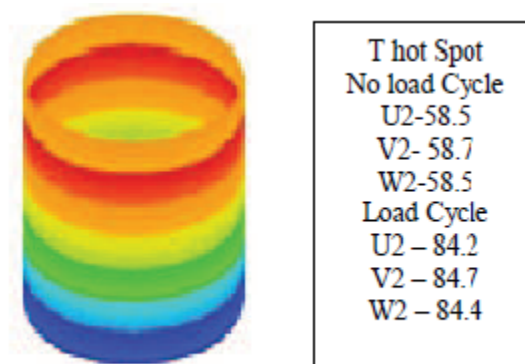Figure 3.16: Temperature Distribution in Primary Winding

Figure 3.17: Temperature Distribution in Secondary Winding

Table 3.11: Temperature Rise of Transformer by Simulation Load Method

Heat Run Cycle	Temperature Rise in $^\circ$ C	
	Primary Winding	Secondary Winding
No load Cycle	7.36	24.91
Load Cycle	57.9	48.11
Total Temperature Rise in $^\circ$ C	61.4	64.4

heat generated by the winding of one particular phase that on the other phases have not been considered.

3.3.6 Results

Based on the above analysis, the transformer has been subjected to heat run test at ERDA, Vadodara, Gujarat, India in accordance to the IS 11171:1985 and IS 2026:2011 by simulation load test method. The summary of the result i.e. the highest value of temperature rise obtained after heat run test has been shown in Table 3.11.

This result indicates that with increase in duct (spacer) size, the air flow in between the primary and secondary winding has increased resulted into better heat transfer through convection. The obtained results are quite close to the one obtained through FEA. It also reveals that the increase in spacer size has effectively increased the resistance of the primary winding resulted into increase in active losses and ultimately the temperature rise. This has been reflected in the final results, the temperature rise of primary (outer) winding for the middle phase is 2.5 $^\circ C$ higher as compared to the achieved results by modified approach. However the same in middle phase of the secondary (inner) winding is differing by just 0.5 $^\circ C$, that too on the lower side.

3.4   Estimation of Magnetizing Inrush Current and Air Clearances

3.4.1   Magnetizing Inrush Current

The magnetization of any induction machine whether it is the transformer or induction motor, leads to the magnetizing inrush currents at the instant of switching. The transient conditions of interest in transformer operation may conveniently be divided into current and voltage phenomena. The former concerns chiefly the switching on of the transformers, while the later is largely concerned with the safety of the insulation on the high voltage side when subjected to voltage surges of very steep wave front at instant t=0+.

It is very often suspected that the failure of the transformer is due to the inrush currents occurring at the instant of its energizing. Although the magnitude of the inrush current may not be as high as the short circuit current under transient condition as it is described in 3.2, study shows that [21]inrush current peaks of 70% of the rated short circuit current cause stresses of the same magnitude as those generated during the short circuit condition.

The inrush current under no-load condition of a transformer can be expressed as in equation 3.38.

$$i_r = (v_s - e_b)/Z \tag{3.38}$$

Where ,

v_s= Supply voltage

e_b= Back emf

Z = Transformer impedance = $\sqrt{\omega L^2 + R^2}$

L = Inductance emf

R = Resistance of the transformer winding

As the transformer works on the flux balancing principle, the back emf or residual flux plays a vital role in determining the value of the inrush current. When the primary side of a transformer is switched on to the normal voltage with the secondary side open circuited (no-load condition), it acts exactly like a simple inductive reactor. At every instant the voltage applied must be balanced by the emf induced by the flux generated in the core by the magnetizing current and by the small drops in resistance and leakage reactance. To a first approximation, it is substantially true that the emf induced must balance the applied voltage. The precise value of the voltage at the instant at which the switch is closed may be anything between zero and its peak value. Further it may be rising or falling and may have either polarity at the switching instant.

If core is initially demagnetized and the switch closes at the peak value of the supply voltage as shown in figure 3.18(a) [119], which occurs twice per cycle, the establishment of emf will be in the opposite direction with the same magnitude of supply voltage which necessitates the flux having maximum rate of change. As a result the flux starts to grow from zero value in the required direction, as also does the magnetizing current. These conditions immediately after the closing of the switch, are, however precisely the same as the final steady state conditions, so that the energizing of the transformer proceeds without any transient. Thus when the transformer is switched on at the instant that the voltage applied passes through a peak value, the voltage, flux and emf waves immediately assume the normal relationship for an inductive circuit.

If the switch closes at the instant that the applied voltage (say completing
the negative cycle and) passes through a zero value as shown in figure
3.18(b) then throughout the first half period the supply voltage is positive
and consequently the emf will be negative (as it is always in phase
opposition to the supply voltage). Accordingly the flux for this half period
must continually increase. It begins at zero value with an increasing slope
or rate of change and finally reaches double its normal peak value at the
end of the first half cycle. This is referred to as the doubling effect. If the
normal magnetizing current is 5 percent of normal rated current, then the
doubling effect may raise it initially to several times the rated current.

This discussion clearly reveals that there will be a variety of possible
circumstances under which a transformer can be suddenly energized: the
switch may close on a voltage of anything between peak value and zero and
correspondingly the severity of the surge of magnetizing current will be
there. Further to this, if there is a residual magnetism in the core then it
may intensify the surge. If the voltage is switched on at a zero in such a
direction so as to augment an existing residual flux, the resultant waveform
of the flux will be as shown in figure 3.18(c). The sinusoid of the flux
variation has still the double amplitude but it is entirely offset from the zero
by the magnitude of the residual flux and rises to the peak.

Hysteresis loops in terms of flux and magnetizing current for all three cases
(a), (b) and (c) are shown in figure 3.18(d). The first case is normal and
symmetrical, the second one is unidirectional and the area of the loop is
actually reduced in spite of the high saturation, however the third curve shows
the super saturated condition which is predominating and the hysteresis loss
is negligible. The peak value of inrush current is very high which can be
expressed by equation 3.39. The value of peak current is mainly governed by
the inductance of the primary winding which is in fact acting as an air cored
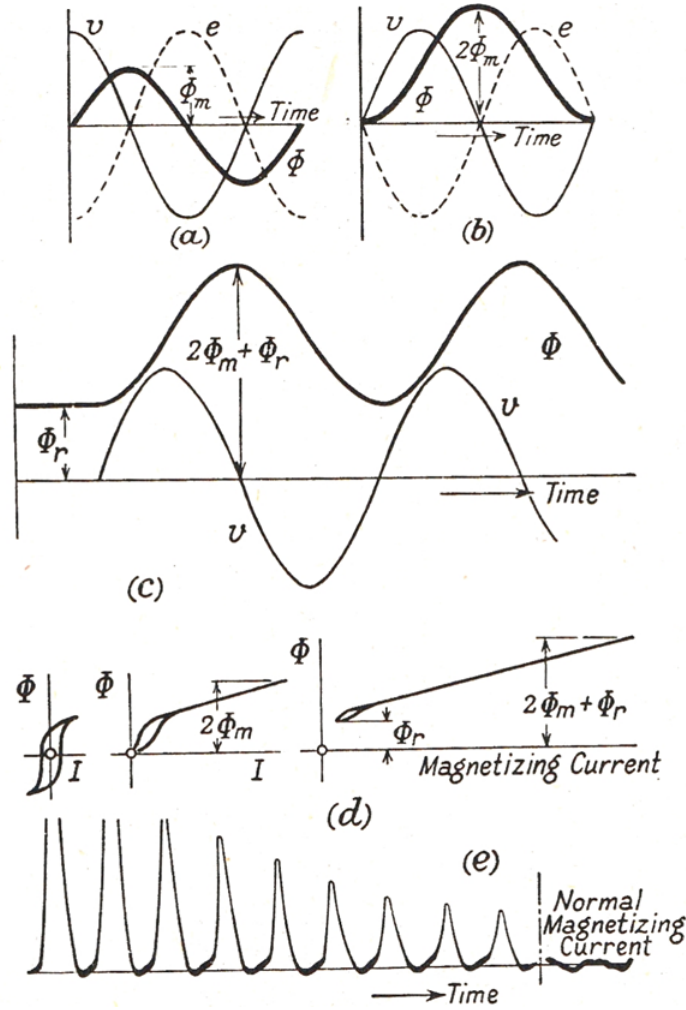
Figure 3.18: Switching In Transients

coil since the core is so saturated that its permeability is just little more than unity. Figure 3.18(e) shows the switching in oscillogram for inrush current which have extended zero pauses. This is due to the great variation with saturation, the negative half cycles are extremely small.

$$I_m = \frac{V_m}{\sqrt{\omega L^2 + R^2}} \left\{ 1 + cos\theta + \frac{\phi_r - \phi_s}{\phi_m} \right\} \tag{3.39}$$

Where

V_m = Peak (maximum) value of the voltage

θ = Angle of switching

ϕ_r= Residual flux in the transformer core

ϕ_s = Flux in the transformer core at the saturation instant

ϕ_m= Peak value of the nominal flux in the transformer core

$$\phi_m = \frac{1}{N} \int_0^t V_m \quad sin\omega t \ dt + \phi_0 \qquad (3.40)$$

ϕ_0 = Residual flux at instant t = 0

This indicates that the magnitude of inrush current depends on the instant
of switching and the presence of residual magnetism within the transformer.
As stated above the peak value of inrush current having magnitude of about
70% of the rated short circuit current produces the similar amount of axial
and radial forces those are produced during the short circuit conditions. This
is because, though the initial high current peaks decay rapidly as the rate of
decay is proportional to the ratio R/L, with R large (due to losses) and L
small (as at the instant of switching the winding acts as an air core reactor),
the distortion of the magnetizing current persists for several seconds till the
flux density falls nearer to the normal raising the inductance value markedly.
This may result into the failure of insulation of the winding due to mechanical
stresses or due to the localize heating if frequent unloaded energization of
the transformer takes place.

The prediction of inrush current though will not relieve the transformer from
its adverse effects will help a designer to counter its effects. Inrush current
can be calculated using equation 3.39 by estimating the value of nominal flux
and its distribution in the transformer core using Finite Element Method.

3.4.2   Air Clearances

The air clearances are not a major problem for low voltage transformers due to availability of the high grade insulating materials now-a-days. However still it's a challenging task for medium voltage and high voltage transformers. For dry type medium and high voltage transformers this problem increases further as air is the only media for cooling and its breakdown strength is strongly governed by the atmospheric pressure and temperature. This necessitates the optimum designing of support insulators for winding with reference to the transformer frame parts and clearances between HV and LV windings and layers of the high voltage winding to avoid earth failures, inter winding failures and inter-turn/inter-layer failures.

Based on the experimental results for uniform magnetic field, the breakdown strength of air is expressed as a power function in terms of atmospheric pressure p and distance d between the live part and earth or between live parts as shown in equation 3.41 [115].

$$V = 24.22 \left(\frac{293pd}{760T} \right) + 6.08 \left(\frac{293pd}{760T} \right)^{\frac{1}{2}} \tag{3.41}$$

Where,
p = Atmospheric pressure in Torr at which breakdown takes place
d = Distance between live part and earth or between live parts in cm
T = Atmospheric temperature in $^\circ K$ at which breakdown takes place

Above equation reveals that at a pressure of 760 torr and room temperature of 20 $^\circ C$ (293 $^\circ K$), the breakdown strength of air will be 30 kV/cm. However this breakdown strength is varying with the atmospheric

conditions. It is highly affected by the humidity and the air density of the surrounding medium. Hence a correction factor for humidity as well as air density is to be applied as given in equation 3.42. This yields an actual breakdown voltage per unit distance.

$$V_a = V \frac{h}{\delta} \tag{3.42}$$

Where,

h = Humidity correction factor

δ = Air density correction factor $= \frac{(273+T_0)p}{(273+T)p_0}$

p_0 = Standard atmospheric pressure = 760 torr

T_0 = Standard atmospheric temperature = 20 $^\circ C$

Since the transformer core geometry is not uniform for all three legs, the magnetic field distribution is also not uniform and hence the breakdown strength of air is highly governed by the concentration of electric field at the winding ends. This demands the estimation of electric field distribution across the winding ends to determine the size of support insulators and clearances between the live parts.

The estimation of electric fields at winding ends using finite element method will help in determining the air clearances as well as the magnetizing inrush current.

3.4.3 Magnetic Field Estimation using FEA

A 3D FEM has been used to determine the potential gradient at various points in a transformer and an inrush current limiting reactor to estimate

the flux distribution and electric field stress for finding the magnetizing inrush current and air clearances.

The magnetic flux density B can be found as the curl of the magnetic vector potential A. To estimate the magnetic vector potential, it has been assumed that the core material is isotropic. Also the displacement current within the core is neglected due to low supply frequency i.e. 50 Hz. The variations in A can be described using equation 3.43 [54].

$$\Delta^2 A - \mu\sigma\frac{\partial A}{\partial t} + \mu J_0 = 0 \tag{3.43}$$

Where,

μ =Magnetic Permeability

σ = Electrical Conductivity

J_0 = Current Density

Using time harmonic mode and representing the magnetic vector potential in complex form, the equation 3.43 reduces to the form in three dimensional Cartesian coordinates as

$$\frac{\partial}{\partial x}\left(\frac{1}{\mu}\frac{\partial A}{\partial x}\right) + \frac{\partial}{\partial y}\left(\frac{1}{\mu}\frac{\partial A}{\partial y}\right) + \frac{\partial}{\partial z}\left(\frac{1}{\mu}\frac{\partial A}{\partial z}\right) - j\omega\sigma A + J_0 = 0 \tag{3.44}$$

The discretization of the domain of study has been done using linear tetrahedron elements. An equation governing each element is derived from the Maxwell's equations directly by using Galerkin approach, as the weighted functions are the same as the shape function - 4 node linear three dimensional tetrahedron element. Accordingly the magnetic vector potential can be expressed as,

$$A(x, y, z) = \sum_{i=1}^{4} A_i N_i \qquad (3.45)$$

Where,

N_i = Element shape function for respective node i = 1,2,3,4

A_i = Approximation of the magnetic vector potential at each node i = 1,2,3,4

Since we have considered linear tetrahedron elements, the shape function can be given as

$$N_i = \frac{1}{6V}(a_i + b_i x + c_i y + d_i z) \qquad (3.46)$$

Where V is the volume of the tetrahedron element expressed as

$$V = \frac{1}{6} \begin{vmatrix} 1 & x_1 & y_1 & z_1 \\ 1 & x_2 & y_2 & z_2 \\ 1 & x_3 & y_3 & z_3 \\ 1 & x_4 & y_4 & z_4 \end{vmatrix}$$

And

$$a_1 = x_4(y_2 z_3 - y_3 z_2) + x_3(y_4 z_2 - y_2 z_4) + x_2(y_3 z_4 - y_4 z_3)$$
$$a_2 = x_4(y_3 z_1 - y_1 z_3) + x_3(y_1 z_4 - y_4 z_1) + x_1(y_4 z_3 - y_3 z_4)$$
$$a_3 = x_4(y_1 z_2 - y_2 z_1) + x_2(y_4 z_1 - y_1 z_4) + x_1(y_2 z_4 - y_4 z_2)$$
$$a_4 = x_3(y_2 z_1 - y_1 z_2) + x_2(y_1 z_3 - y_3 z_1) + x_1(y_3 z_2 - y_2 z_3)$$

$$b_1 = y_4(z_3 - z_2) + y_3(z_2 - z_4) + y_2(z_4 - z_3)$$
$$b_2 = y_4(z_1 - z_3) + y_1(z_3 - z_4) + y_3(z_4 - z_1)$$

$$b_3 = y_4(z_2 - z_1) + y_2(z_1 - z_4) + y_1(z_4 - z_2)$$
$$b_4 = y_3(z_1 - z_2) + y_1(z_2 - z_3) + y_2(z_3 - z_1)$$

$$c_1 = x_4(z_2 - z_3) + x_2(z_3 - z_4) + x_3(z_4 - z_2)$$
$$c_2 = x_4(z_3 - z_1) + x_3(z_1 - z_4) + x_1(z_4 - z_3)$$
$$c_3 = x_4(z_1 - z_2) + x_1(z_2 - z_4) + x_2(z_4 - z_1)$$
$$c_4 = x_3(z_2 - z_1) + x_2(z_1 - z_3) + x_1(z_3 - z_2)$$

$$d_1 = x_4(y_3 - y_2) + x_3(y_2 - y_4) + x_2(y_4 - y_3)$$
$$d_2 = x_4(y_1 - y_3) + x_1(y_3 - y_4) + x_3(y_4 - y_1)$$
$$d_3 = x_4(y_2 - y_1) + x_2(y_1 - y_4) + x_1(y_4 - y_2)$$
$$d_4 = x_3(y_1 - y_2) + x_1(y_2 - y_3) + x_2(y_3 - y_1)$$

The method of the weighted residue with Galerkin approach is then applied to the differential equation 3.44 where the integrations are performed over the element domain - v.

$$\int_v N_i \left(\frac{\partial}{\partial x} \left(\frac{1}{\mu} \frac{\partial A}{\partial x} \right) + \frac{\partial}{\partial y} \left(\frac{1}{\mu} \frac{\partial A}{\partial y} \right) + \frac{\partial}{\partial z} \left(\frac{1}{\mu} \frac{\partial A}{\partial z} \right) \right) \partial v$$
$$- \int_v N_i j \omega \sigma A \partial v + \int_v N_i J_0 \partial v = 0 \tag{3.47}$$

The solution to the equation 3.47 yields magnetic field distribution across the domain of interest.

Figure 3.19: 1.5 kVA Single Phase Transformer

3.4.4   Case Studies and Results

3.4.4.1   Determination of Inrush Current

Measurement of inrush current in a large rating transformer is practically difficult. Hence a small transformer of 1.5 kVA rating having parameter as shown in table 3.12 has been taken as a reference case - to estimate the inrush current and time duration for which it lasts using FEM.

Table 3.12: Specifications of 1.5 kVA Transformer

Primary Voltage	415 V
Secondary Voltage	230 V
Frequency	50 / 60 Hz
Insulation Class / Temperature Rise	F / F (90° C)
Dielectric Level	3 kV / Min

The numbers of elements in the entire domain of the transformer were 36000 each having a shape function of a 4 node tetrahedron. The boundary condition was kept to have electric field strength value $\leq$ 0.1 kV/mm. The

Table 3.13: Inrush Current

Estimated Parameters for Inrush Current using FEA		Measured Parameters	
Inrush Current in A	Time Duration in Cycle	Inrush Current in A	Time Duration in Cycle
105	3	112.2	2
		116.42	1
		116.26	1
		117.39	1
		118.71	1
		116.23	1

violation of boundary condition during any stage of FEA, demands the redesign of the transformer to avoid excessive inrush current and consequently the failure of the transformer.

The estimated value and measured values of inrush current at different switching instances are summarized in table 3.13 below. The measurement of inrush current was carried out at ERDA Vadodara using peak current detector.

3.4.4.2   Determination of Air Clearances

The air clearances have been identified using FEA for an air core medium voltage reactor (figure 3.20) being used as an inrush current limiter for 11 kV 250 HP drive motor. The specification of the reactor are shown in table 3.14 below. The reactor is to be designed to limit the inrush current of the motor and hence is being directly subjected to the transient current at the instant of switching. The duty cycle of the reactor is just for 3 seconds but during this time duration there must not be any inter – turn / inter layer failure. For the same reason, the reactor was to be tested for an impulse level of 60 kV peak in line with IEC 60076 part 6, 2011.

Table 3.14: Specifications of Inrush Current Limiting Reactor

Power Rating	280 kVAR
Inductance	430 mH $\pm$ 5%
Frequency	50 / 60 Hz
Nominal System Voltage	11 kV
Type of Reactor / Duty Cycle	Air Core / Intermittent (3 Sec ON)
Insulation Class / Temperature Rise	F / F (90° C)
Dielectric Level	28 kV/Min
Impulse Level	60 kV Peak

Figure 3.20: 280 kVAR Air Core Reactor

Table 3.15: Electric Field Strength at Winding Ends of Inrush Current Limiting Reactor

FEA First Run		TFEA Second Run	
Air Clearances Between Two Consecutive Layers in mm	Obtained Value of Electric Field Strength at winding ends	Air Clearances Between Two Consecutive Layers in mm	Obtained Value of Electric Field Strength at winding ends
5 mm with uniform height of each layer	3.5 kV / mm	12 mm with unequal height of alternate layers	1.8 kV / mm

The numbers of elements in the entire domain of the reactor were 96000 each having a shape functions of a 4 node tetrahedron. The boundary condition was kept to have electric field strength value $\leq$ 2 kV/mm. The analysis using FEM was carried out first by keeping the air clearances of 5 mm between two consecutive layers with equal height of each layer. The field distribution was obtained showing the electric field strength as given in table 3.15 which violated the boundary condition. Hence the air clearances have been increased from 5 mm to 12 mm with having non uniform layer heights at alternate layers. This has substantially reduced the electric field strength at winding ends.

The reactor is then subjected to the impulse testing at ERDA which successfully withstood the test in line with IEC 60076-6, 2011.

Based on the above results, the air clearances have been worked out for different system voltages (voltage level > 1.2 kV and up to 12 kV) as summarized in table 3.16.

The above values are with consideration of air density and humidity correction factors. However the altitude considered is less than 1000 m.

Table 3.16: Nominal Air Clearances for Various System Voltages Up to 36 kV Class

System Voltage in kV	Minimum Air Clearance in mm	
	Between Winding and Frame	Between Phase Windings
≤ 3.6	30	15
≤ 7.2	50	20
≤ 12.0	100	35

3.5   Conclusion

The findings of this chapter can be summarized as under.

1. The short circuit stresses can be evaluated in terms of mechanical deformation using finite element method to an extent whereby considering proper factor of safety, the short circuit proof equipment (reactor in this case) can be built for a specified short circuit level. This approach is accurate, less time consuming and helps in identifying the factor of safety without developing any prototype model for verification of impedance value. A reverse calculation can be done to finally estimate the impedance value. The same approach can be extended to determine the short circuit withstands level of other electrical equipments such as power transformer for high and ultra high voltage levels, generators, motors etc. The method can be used to identify the inter layer forces between the layers of a concentric winding machine. Also the deformation in a winding can be predicted under transient condition especially in case of large power and distribution transformers.

2. The thermal behavior of dry type transformers can be estimated quite accurately with the help of 3D finite element method using Variational approach as compared to 2 dimensional approaches. This helps in adopting proper designing approach (safety factor) whereby the

required level of temperature rise (thermal class) can be achieved. This consumes less time and helps in determining the safety factor without any physical development of prototype model. The approach can further be extended to find out the thermal behavior of other electrical equipments such as generators, motors, oil cooled transformer, etc. This approach can even be modified to have higher accuracy in the results obtained either by selecting eight node break elements with each of the nodes having three translational degrees of freedom in the nodal x, y and z directions or with elements having even higher than eight nodes especially for the analysis of large power and distribution transformers or other equipments.

3. The magnetizing inrush currents and air clearance can be approximated to a quite close approximation using 3 dimensional Finite Element Method. This will help in optimizing the design without an actual build up of a prototype model. The approach can be extended for the estimation of electric field while the equipments are subjected for the operations at higher altitude also.